Supplementary Material

Characterisation of Shock Waves in Power Ultrasound

Mohammad Khavari, Abhinav Priyadarshi, Andrew Hurrell, Koulis Pericleous, Dmitry Eskin
Iakovos Tzanakis

1 FOH Sensitivity

A fibre-optic hydrophone (Precision Acoustics, Ltd.) was calibrated by the manufacturer for a high-frequency range of $1 - 30$ MHz. Figure S1 shows the sensitivity of the probe for this range. The red spots are the calibrated data points for each discrete step and the blue line shows the interpolated values used for other frequencies.

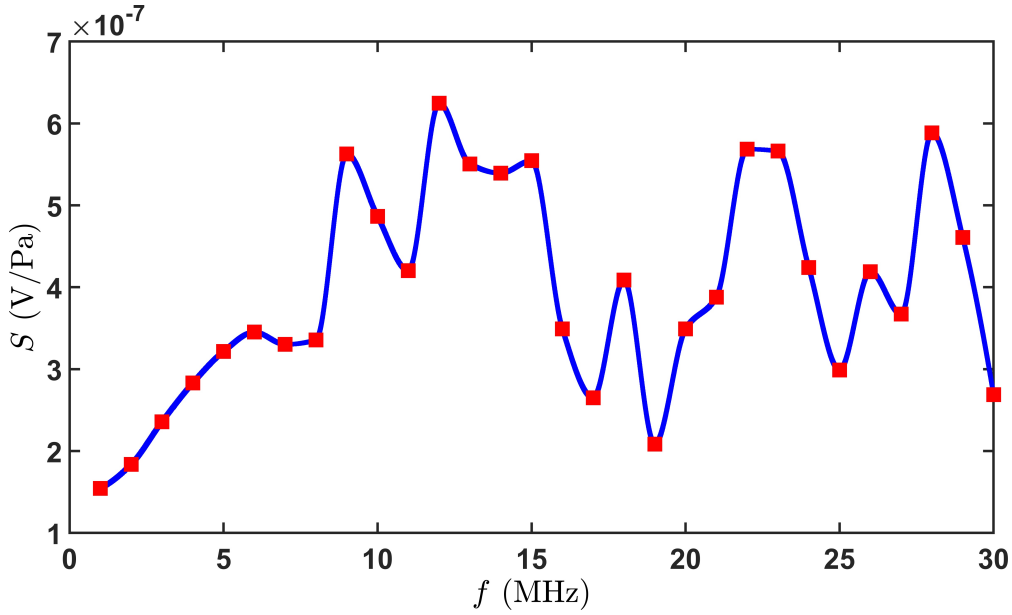

Figure S1: Sensitivity of the FOH vs. frequency (Precision Acoustics, Ltd.).

2 Deconvolution Process

Figure S2 summarizes the deconvolution process in each step for input power of 60%, $x = 0$ and $y = 1$ mm. To find the pressure in the time domain, we first subtracted the noise from the original acquired voltage data points, applied a bandpass filter for the FOH calibrated range ($1 - 30$ MHz) and then calculated the Fast Fourier Transform of the resultant signal. Then the signal is converted into a single-sided spectrum, divided by the probe sensitivity (figure S1) and converted back to double-sided spectrum. Finally, the pressure in time domain is found by applying the inverse Fast Fourier Transform to the signal. Figure S2(a) shows the original voltage reading ($V - t$). Figure S2(b) shows the Fast Fourier Transform of this signal with the inset plot showing the effect of the bandpass. Note how the filter suppresses the peak at the driving frequency (24 kHz). Figure S2(c) shows the resultant pressure in frequency domain after dividing by sensitivity. We again plot the signals with and without filter to show how the data outside the probe calibration range ($1 - 30$ MHz) are ignored. Finally, figure S2(d) shows the final signal as the pressure in time domain for a single waveform from which we calculated the $P_{\max}$ and P_{RMS}. Our experimental results show that as the input power increases, we observe a smaller number of prominent peaks in the $P - t$ profile (figure S2(d)) though with higher pressure amplitude (figure S3) and therefore, the time between those peaks increases. This may be attributed to cavitation shielding, extended periods of non-collapsing deflations and distribution of shock energy to other lower band frequencies (see relevant discussion to figure 4).

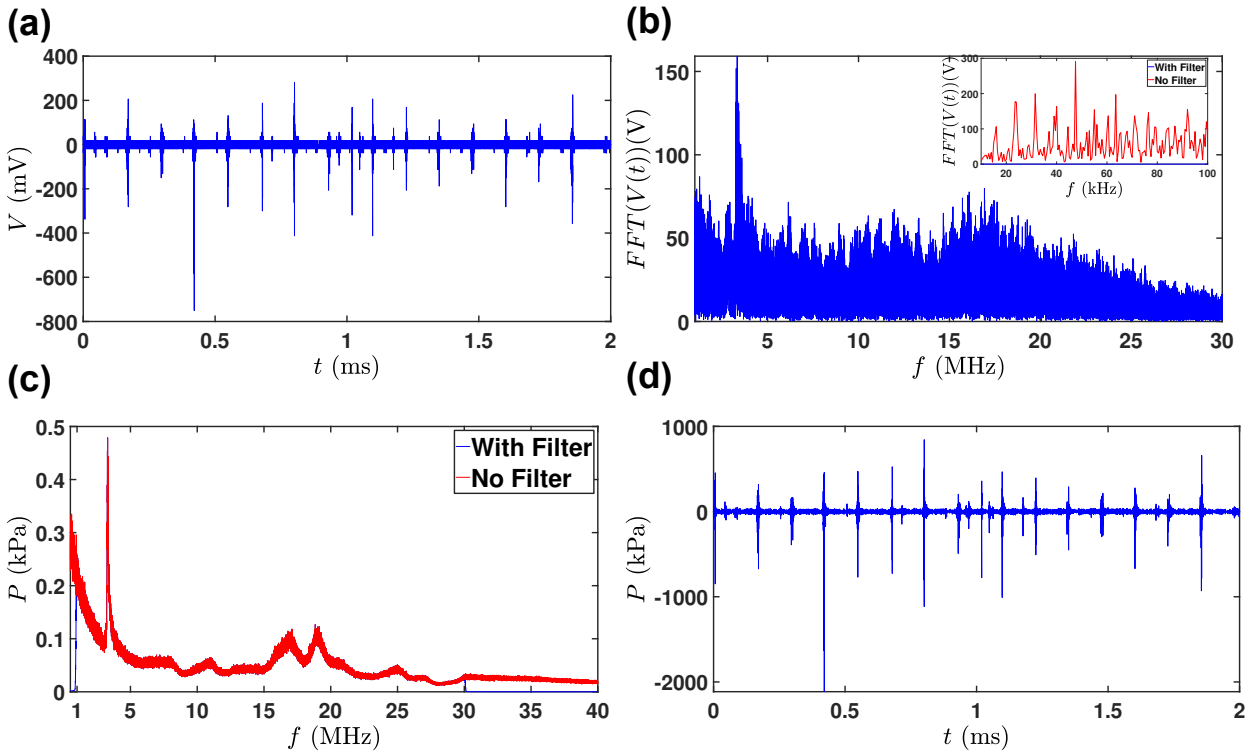

Figure S2: The deconvolution process: a) Raw voltage signal. b) Fourier Transform of voltage signal. The inset shows the magnified plot near the driving frequency with and without the bandpass filter. Note how the peak at $f_0 = 24$ kHz is suppressed. c) Pressure in frequency domain with and without filter. Note the effect of filtering at both ends of the calibration range ($1 - 30$ MHz). d) Final output of the deconvolution process as pressure in time domain for one waveform. These are obtained for input power of 60%, $x = 0$ and $y = 1$ mm.

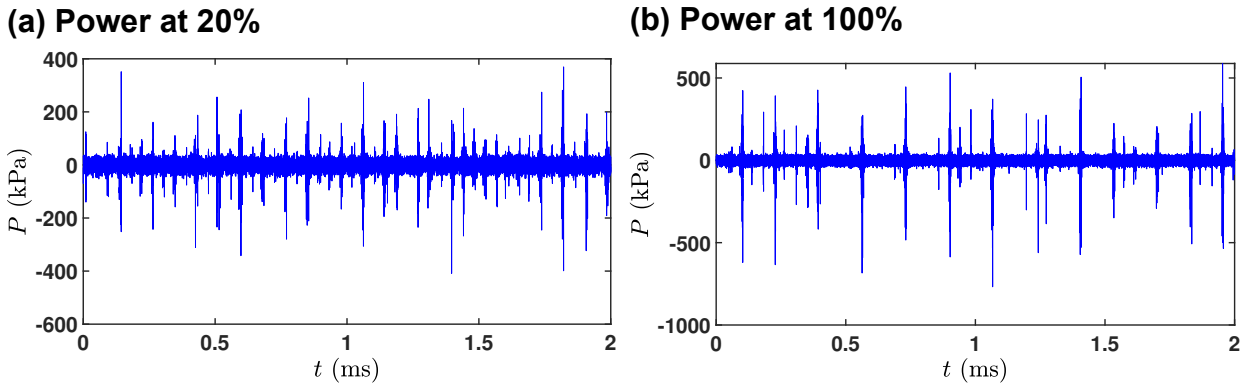

Figure S3: Comparison of pressure distribution in time domain for the same position ($x = 3$ and $y = 2$ mm) and two input powers: a) 20% and b) 100%.

3 Effect of a Different Transducer and Sonotrode Size

To confirm the independence of the observed peak of the transducer and the sonotrode diameter, we performed a few experiments with another transducer (Hielscher, UIP500hdT, 20 kHz) with a much bigger sonotrode tip ($d_s = 22$ mm). The acoustic cavitation created by the second sonotrode also creates the peak at the same range of frequencies, with a bigger amplitude (compared to our main sonotrode for the same position). Figure S4 and S5 show the comparison of the pressure in frequency domain for both sonotrodes for the same position ($x = 0, y = 5$ mm) for two input powers (20% and 60%). The inset plots show the proximal region of the peak. Note that we used the same FOH probe for these measurements. Table S1 exhibits the maximum and RMS pressure magnitudes for these cases. Therefore, higher transducer power and larger sonotrode diameter will lead to higher peak pressure amplitude.

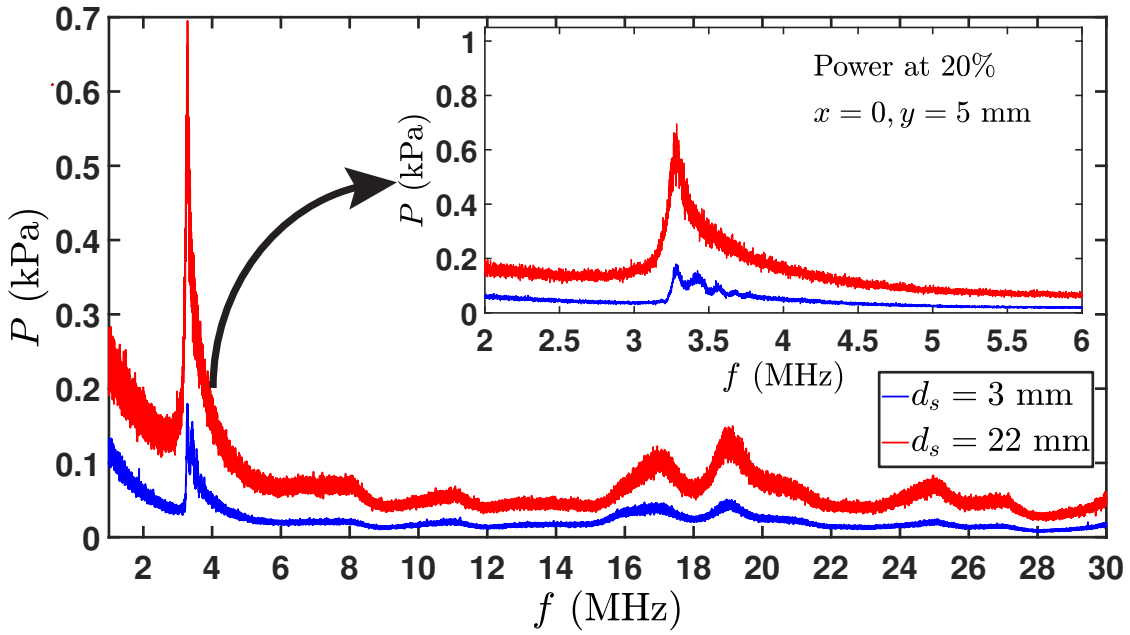

Figure S4: Pressure vs. frequency measured by the same FOH probe for two different transducers (and different sonotrodes) for the same position ($x = 0, y = 5$ mm) and input power of 20%. The pressure was averaged over 60 waveforms. The inset plot magnifies the region of the peak in question.

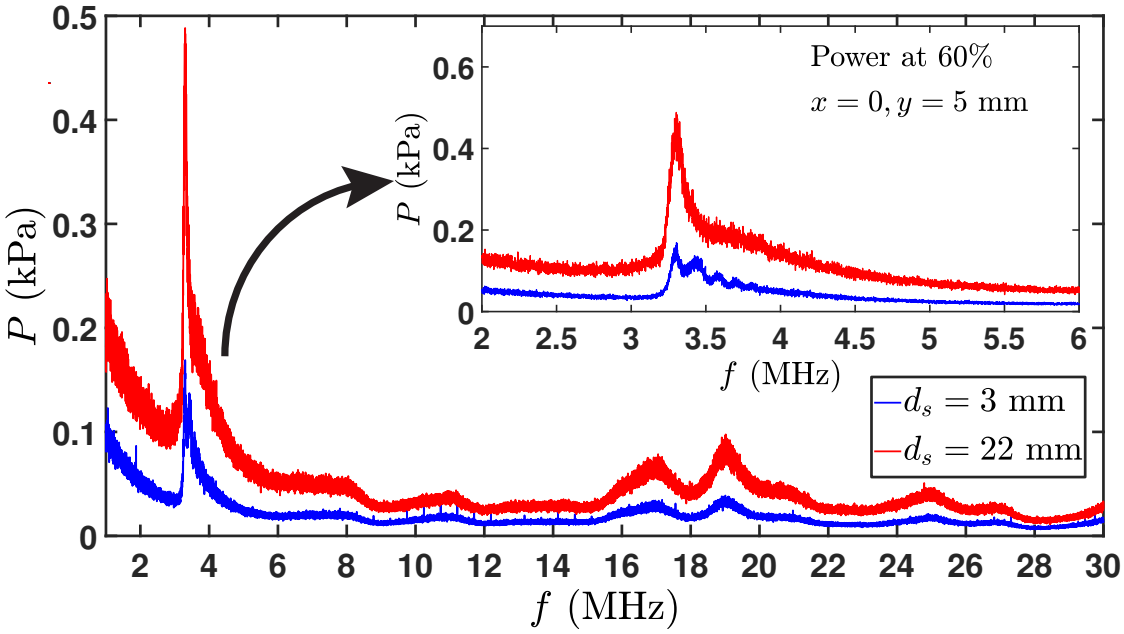

Figure S5: Pressure vs. frequency measured by the same FOH probe for two different transducers (and different sonotrodes) for the same position ($x = 0, y = 5$ mm) and input power of 60%. The pressure was averaged over 60 waveforms. The inset plot magnifies the region of the peak in question.

Table S1: Comparing the maximum and RMS pressures for two different sonotrodes and two different input powers for the same position ($x = 0, y = 5$ mm). The pressure values are averaged over 60 waveforms (of 2 ms each, see figure S2(d)) for the calibration range ($1 - 30$ MHz).

	$P_{\max}$ (kPa)		P_{RMS} (kPa)	
	Power at 20%	Power at 60%	Power at 20%	Power at 60%
Sonotrode 1 ($d_s = 3$ mm)	222.5	189.1	12.2	10.5
Sonotrode 2 ($d_s = 22$ mm)	1213.8	1205.9	36.7	26.2

4 Effect of a Different FOH Sensor

We performed several experiments with our main transducer (24 kHz, 3 mm sonotrode) and a second FOH sensor (Precision Acoustics Ltd.) having its own calibration over the exact same range ($1 - 30$ MHz). The experiments were carried out for several different positions and input powers. The peak at the same frequency range was observed for all cases. Figure S6 shows the pressure profile in frequency domain for the second probe and compares it with the main sensor for the same position ($x = 3$ mm,$y = 3$ mm) and input power of 20%. The peak is clearly observed for the second probe as well, occurring at the same range of the first probe.

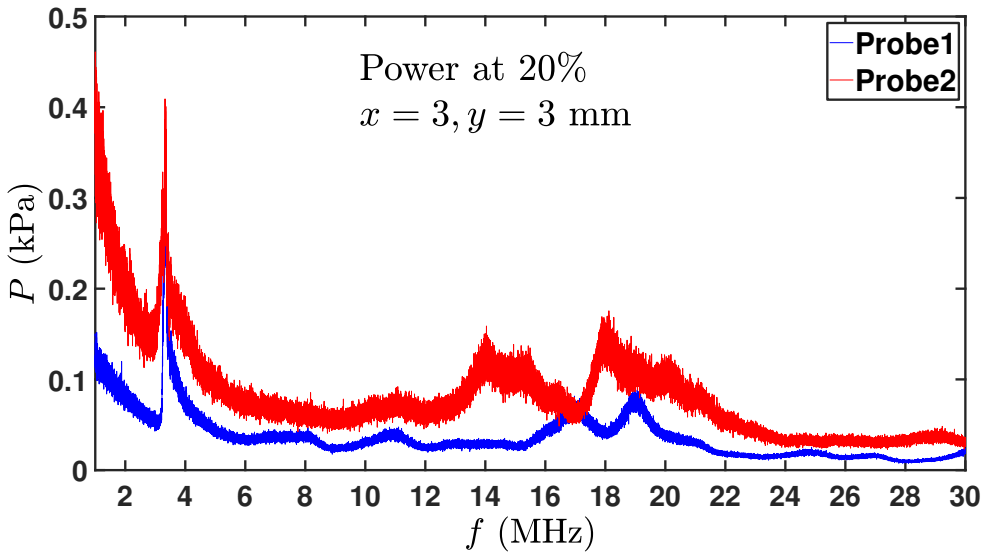

Figure S6: Pressure vs. frequency measured by two different FOH probes for the same position ($x = 3, y = 3$ mm) and input power of 20%. The pressure was averaged over 60 waveforms.

5 Effect of Glass Walls

To further confirm that the observed peak was due to shock wave propagation, we performed several experiments in different configurations. Figure S7 shows the results for these cases. The inset schematics show the top view of the glass tank and display how the probe and sonotrode are positioned. First, we placed the sonotrode and FOH probe in separate compartments (each filled with water) and different lines at the furthest possible distance (180 mm). Figure S7(a) shows how the insertion loss of these glass walls (separating the probe and sonotrode) leads to the suppression of the peak at ∼3.3 MHz. Figure S7(b) shows a similar configuration, except that this time the probe and sonotrode are on the same line, but still in separate compartments. The peak is once again significantly collapsed. For these two cases, we used our main 24 kHz transducer (UP200S with 3 mm tip diameter). We then placed the FOH probe and sonotrode at the two far corners (figure S7(c)) of the glass tank and used our stronger transducer (Hielscher, UIP500hdT) with bigger sonotrode (22 mm). All other compartments were also filled with water for this case. The input power for all cases was 20%. As seen from the figure S7(c), because of the suppression of the ultrasonic cavitation in this long distance and the losses due to the presence of the glass walls, the peak is completely disappeared. All these experiments further imply that the observed peak at ∼3.3 MHz could be related to shock wave emission.

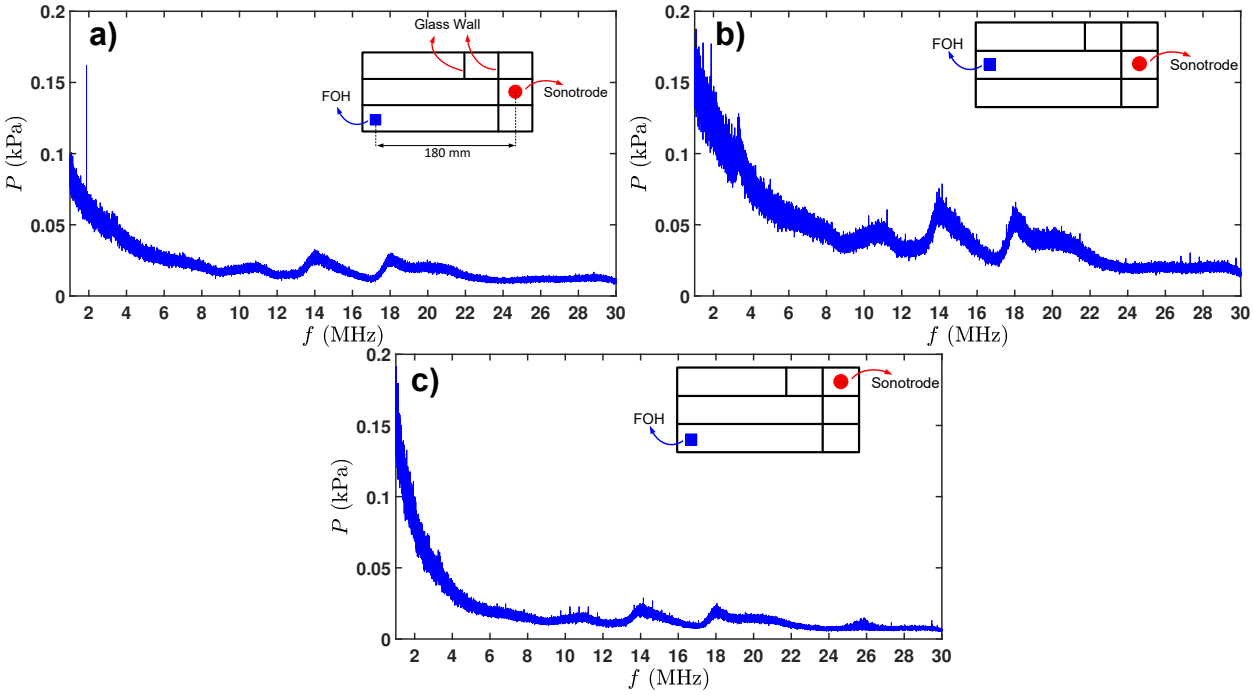

Figure S7: Pressure vs. frequency for different configuration of sonotrode and FOH probe. The inset schematics (the top view of the glass tank) show how they are positioned: a) sonotrode and probes at two separate compartments and different lines; b) sonotrode and probe at two different compartments but on the same line and c) sonotrode and probe at two far corners of the glass tank, with all other compartments filled with water. For all cases, input power was 20%. For (a) and (b), we used our main transducer (24 kHz, 3 mm tip) and for (c), we used the powerful transducer (22 mm tip). The pressure was averaged over 60 waveforms.

6 Effect of Electromagnetic Interference

Eventually, to eliminate the role of electromagnetic interference, we did a few experiments with the probe tip being covered with an air-filled finger cot (the air/water boundary is acoustically reflective). As seen from the result shown in figure S8, the peak is no longer present.

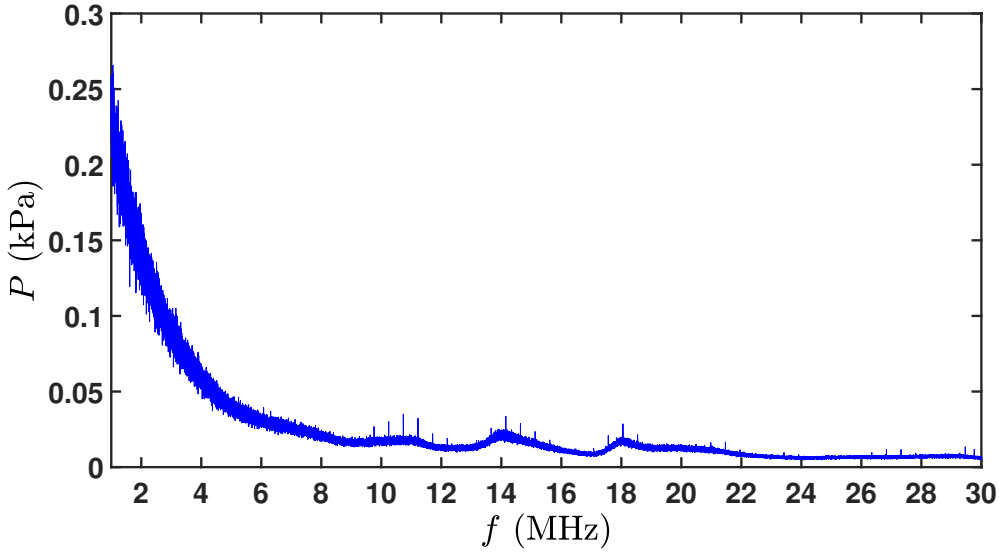

Figure S8: Pressure vs. frequency for a case where the probe tip was covered with an acoustically reflective material. The peak is no longer present. We used our main transducer (24 kHz), main glass tank and second probe for this case. Input power was 100% and the distance between probe and sonotrode was 30 mm.

7 Effect of Filtering the Peak Frequencies

We propose that the observed peak might be associated with the shock wave. To see the relation between this peak and overall shock-wave energy, we applied an additional bandpass filter within the range containing the peak ($3-4$ MHz) to remove the contents of these frequencies. Figure S9(a) shows the pressure vs. frequency plot with and without this filter, clearly showing how the filter suppresses the information within this range (see the inset plot for magnified region). Figure S9(b) shows the pressure profile in time domain for both cases (with and without filter) for a single waveform depicting a drop in peak pressure magnitudes. This drop is around $25\% \pm 6\%$. This indicates that the observed peak contains some of the shock wave power, however most of its energy is, as expected, distributed among all other frequencies (broadband noise). These results are obtained for the studied case in figure 2, i.e., the probe was placed at $x = 0$ and $y = 1$ mm and input power was 60%.

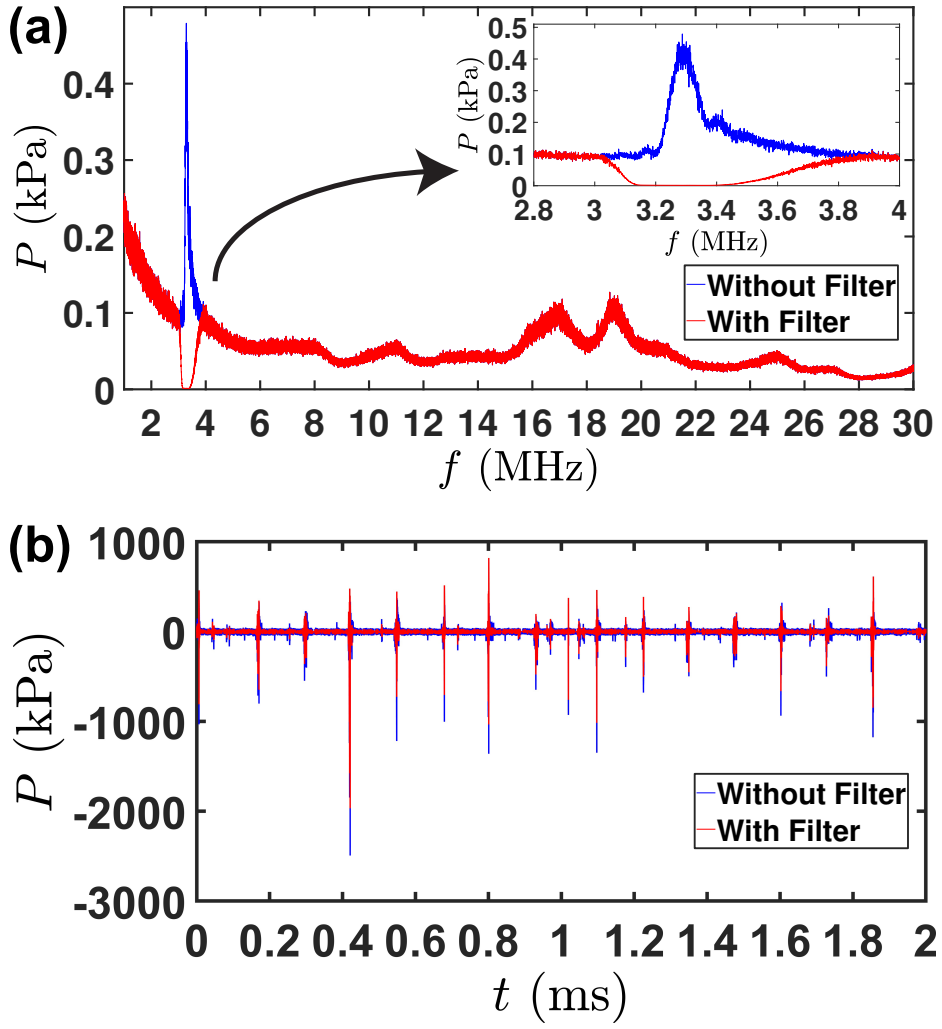

Figure S9: The effect of applying an additional bandpass filter on $3-4$ MHz (the frequency range containing the peak). a) Pressure vs. frequency for both with and without this filter for the entire calibrated range. Inset: magnified zone of the filtered range clearly showing how the additional filter suppresses the data within this range. b) The resultant $P-t$ plot for both with and without filter. The peak pressure magnitudes for the filtered data are dropped. The probe was at $x = 0$ and $y = 1$ mm and input power was 60%. The pressure at (a) was averaged over 60 waveforms. The pressure distribution at (b) is for one waveform.

8 Shock Wave Frequency from High-Speed Imaging

Figure S10 shows the measured frequency for numerous shock waves (around 300) at different time stamps from six different experiments. For each case, several measurements were performed for the wavelength (and frequency), the average of which is also shown in the legend. The mean frequency of all experiments was 4.78 ± 0.3 MHz which is in the same order though $\sim 30\%$ off to the calculated value from the deconvolution process of pressure measurements. The tolerance in the measurements from the high-speed recordings are due to the image resolution (pixel size 39.02 ± 4 μm) and measurement of the speed of emission (speed of shock wave 1464 ± 5 m/s).

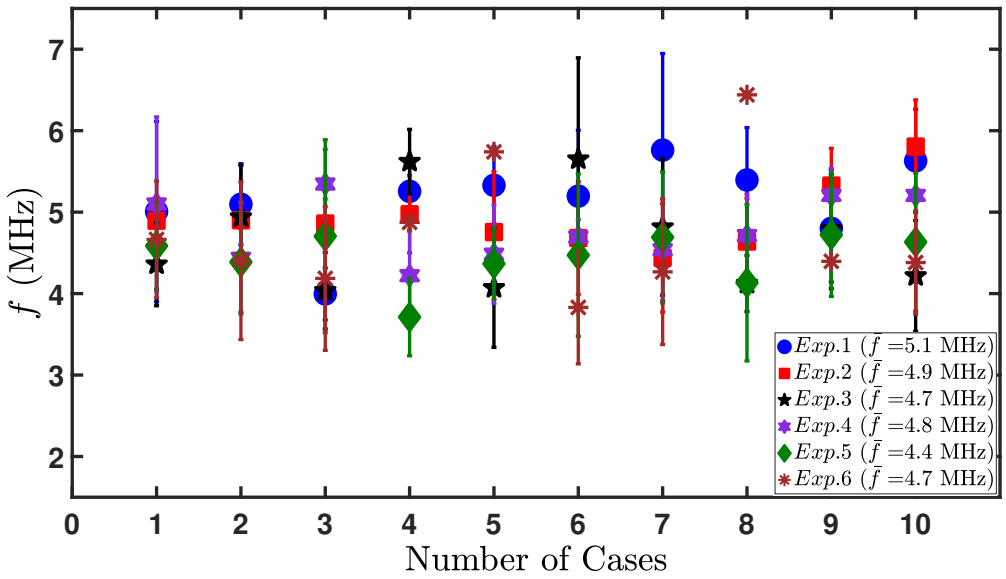

Figure S10: Frequency of the shock wave emission from high-speed recordings for different experiments. The frequencies in the legend are the mean frequency for each experiment.

We suspect the reason for this discrepancy lies on the selected approach for identifying the borders of the spatially propagating shock waves. For all the shock waves, the frequency was determined by the analysis of the wave pattern captured by the high-speed recordings and the corresponding measured wavelength (see figure S11). For the sake of consistency and clarity, for all the 300 cases, we decided to use two distinct points (points a and b in figure S11) as the absolute borders of the studied shock waves which indicate a well-defined sinusoidal or so-called N-wave (figure S11(b)), associated with propagation of shock waves. However, as shown in figure S11, careful visual inspection by scrutinizing the individual pixel intensity revealed that the borders of the shock waves (bow to tail) are not within the designated area defined initially (blue dash arrow and distance s_1 in figure S11(b1) and (b2)) that corresponds to the waveform of figure 3(b), but they extend, on average, by 1-2 pixels. For the case of figure S11, this extension is by 1 pixel in the tail (see figure S11(c1) where the red solid arrow and distance s_2 indicate the actual borders of the shock wave). This corresponds to a much larger wavelength as indicated by figure S11(c2) (points a_0 and b). This discrepancy may well occur due to the fluid turbulence that can generate artefacts in bows and tails of the shock wave as shown in (Haering Jr, Smolka et al. 2006). This will affect the diffraction of light and pixel contrast and therefore prevent a perfect distinction of the borders of the shock wave. These larger wavelengths will drop the average values of frequency in figure S10, bringing them closer to the frequencies measured by the FOH probe ($3.27 - 3.43$ MHz).

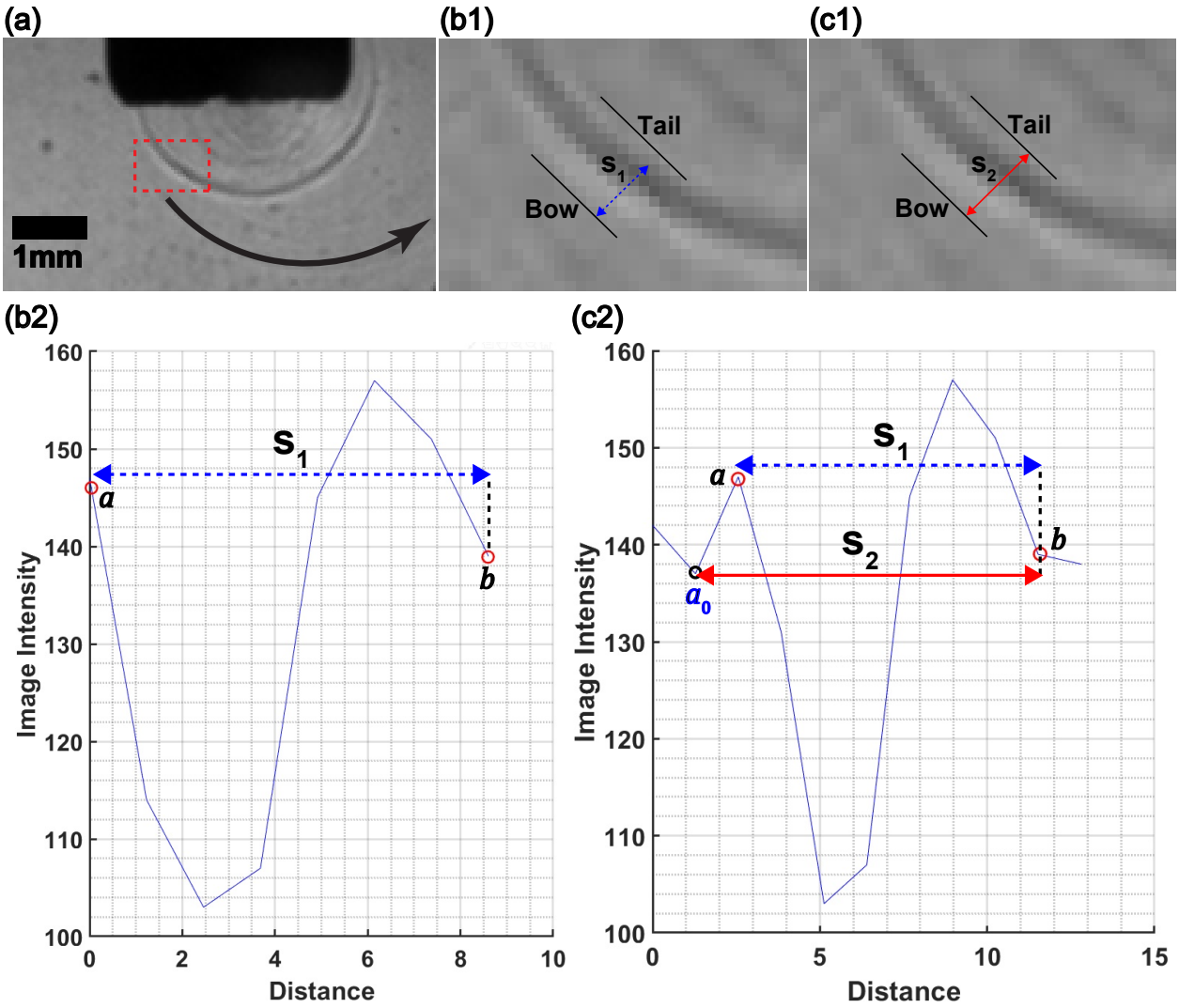

Figure S11: a) Shock wave around the sonotrode; b1) Magnified area near the shock wave with its bow and tail, corresponding intensity profile (b2) and the selected distance (s_1) considered for wavelength measurement; c1) The same case with the actual distance (s_2) and its intensity profile (c2). Blue (colour online) dash arrow is the selected distance (s_1) for measuring the wavelength and red solid arrow is the actual distance s_2 being 1-2 pixels larger than s_1.

9 Effect of Input Power

Figure S12 and S13 show the contour plots of $P_{\max}$ and P_{RMS} vs. input power and vertical position from the sonotrode for four different horizontal positions. These results belong to the right side of the sonotrode. For small x (< 2 mm), the pressure does not depend much on the input power for $y = 1 - 4$ mm, while far from the sonotrode, the pressure increases as the input power is raised, thus shock wave impact would be more effective in the vicinity of the source.

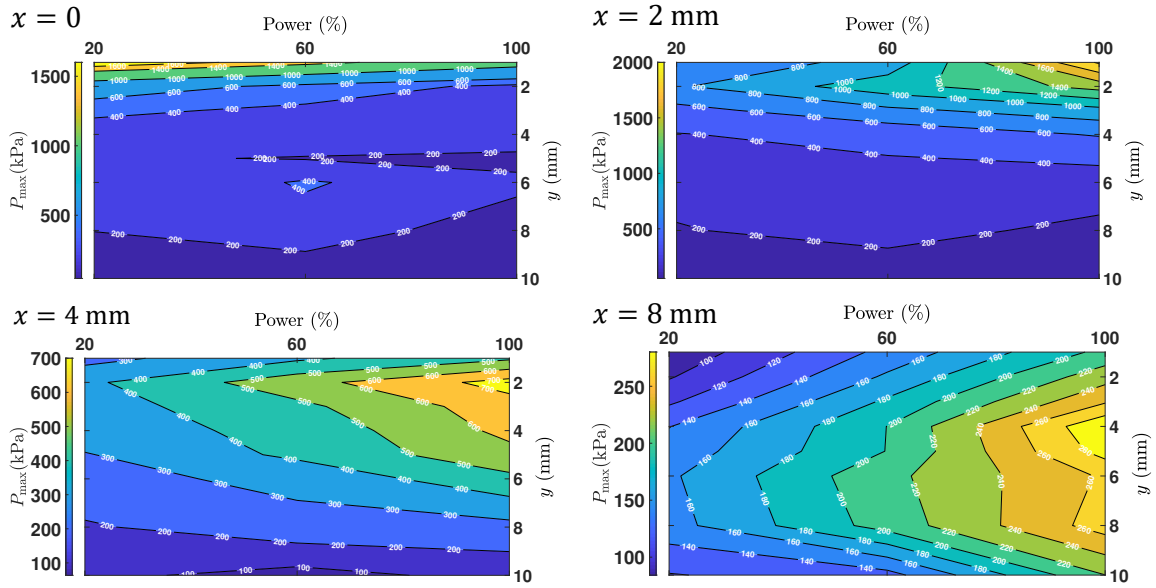

Figure S12: Contour plots of $P_{\max}$ vs. input power and vertical position for 4 different horizontal positions on the right side of the sonotrode.

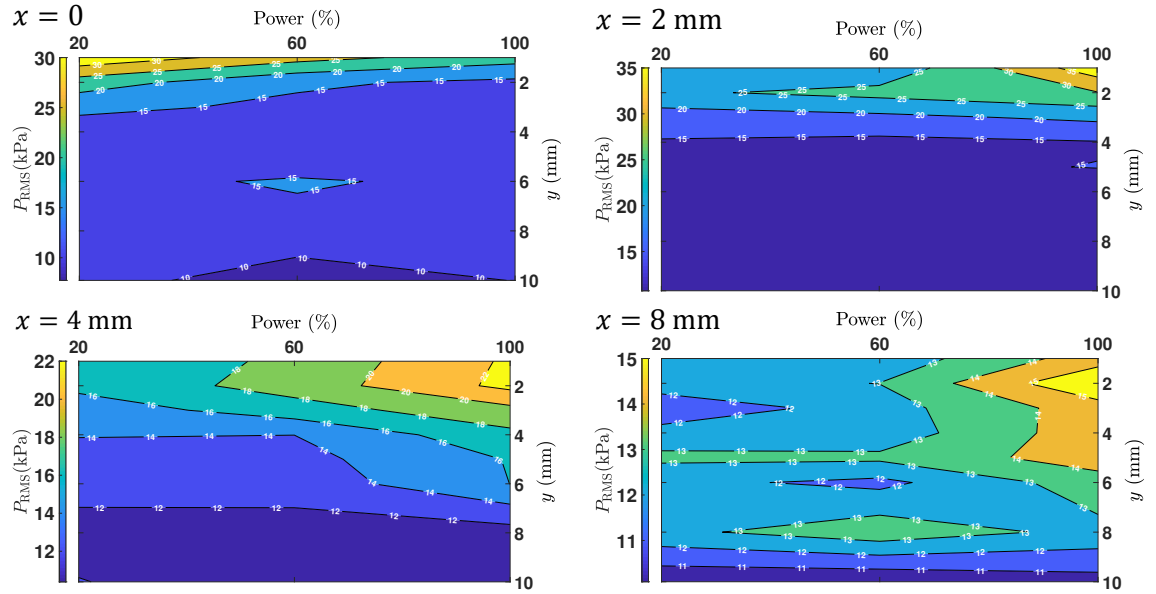

Figure S13: Contour plots of P_{RMS} vs. input power and vertical position for 4 different horizontal positions on the right side of the sonotrode.

10 Peak Frequency

The dependence of the peak frequency on position for two other input powers of 60% and 100% are shown in figure S14 and S15 respectively.

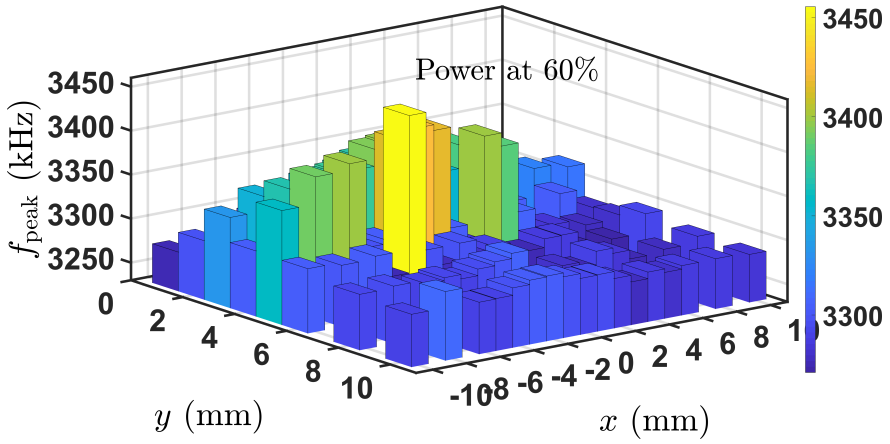

Figure S14: 3D distribution of the peak frequency vs. horizontal and vertical positions for transducer power of 60%.

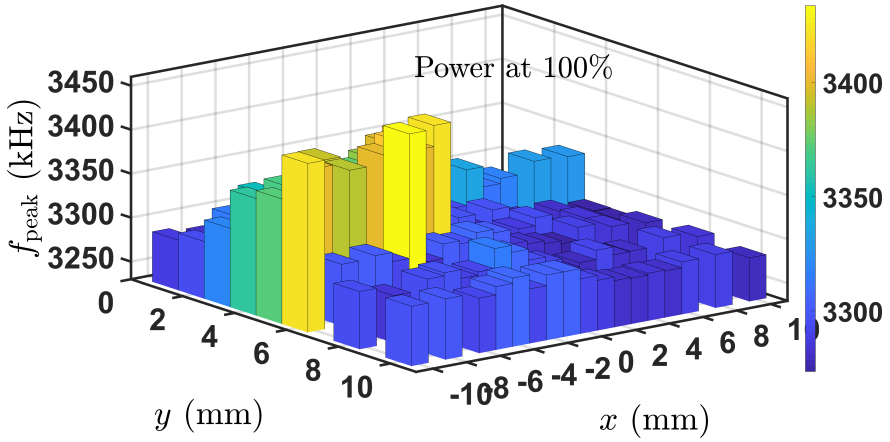

Figure S15: 3D distribution of the peak frequency vs. horizontal and vertical positions for transducer power of 100%.

Table S2: Minimum and maximum magnitudes (of all positions) of the peak frequency and peak pressure for three different input powers. The pressure values are averaged over 60 waveforms.

	f_{peak} (MHz)		P_{peak} (kPa)	
	Min	Max	Min	Max
Power at 20%	3.27	3.4	0.124	0.715
Power at 60%	3.27	3.46	0.125	0.946
Power at 100%	3.27	3.43	0.156	1.16

11 dB Scale

Figure S16 shows the acoustic level in dB scale vs. frequency (for low frequency range) for the case study presented in the manuscript. The probe was at x=0 and y=1 mm and input power was 60%. Note that for this plot, the bandpass filter is not applied, since this low frequency range is outside the calibrated range of FOH. For this plot, we used a fixed value for sensitivity (sensitivity at 1 MHz). The probe is capable of detecting the driving frequency and its harmonics, ultra- and sub-harmonics as indicated by the arrows in figure S16.

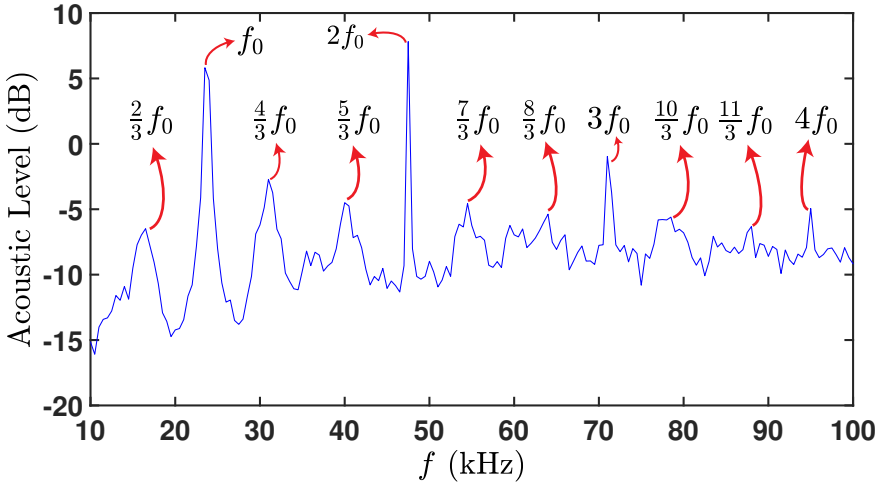

Figure S16: Acoustic spectrum level (dB) vs. frequency (without bandpass filter) for $x = 0$ and $y = 1$ mm and input power of 60%. The pressure was averaged over 60 waveforms. Along with the driving frequency (24 kHz), the probe detects its harmonics, ultra- and sub-harmoncis.

Reference

Haering Jr, E. A., J. W. Smolka, J. E. Murray and K. J. Plotkin (2006), Flight Demonstration Of Low Overpressure N-Wave Sonic Booms And Evanescent Waves, AIP Conference Proceedings, American Institute of Physics.